Hindawi
Journal of Engineering
Volume 2024, Article ID 8866265, 13 pages
https://doi.org/10.1155/2024/8866265

*Research Article*

# Effects of Thermal Radiation and Variable Porosity on Unsteady Magnetoconvective Heat-Mass Transport Past a Vertical Perforated Sheet

**Md. Abu Bkar PK,[1] Md. Hasanuzzaman,[2] Md. Mosharof Hossain,[3] and Dipayan Mondal[4]**

[1]*Department of Applied Mathematics, University of Rajshahi, Rajshahi 6205, Bangladesh*
[2]*Department of Mathematics, Khulna University of Engineering & Technology, Khulna 9203, Bangladesh*
[3]*Department of Mathematics, Bangladesh University of Engineering & Technology, Dhaka 1000, Bangladesh*
[4]*Department of Mechanical Engineering, Khulna University of Engineering & Technology, Khulna 9203, Bangladesh*

Correspondence should be addressed to Md. Hasanuzzaman; hasanuzzaman@math.kuet.ac.bd

Received 5 October 2023; Revised 25 December 2023; Accepted 16 January 2024; Published 29 January 2024

Academic Editor: Yongping Chen



This study interprets the effects of radiative and variable porosity on a time-dependent MHD-free convective heat-mass transfer past a vertical porous sheet. The PDEs governing the research are converted into nondimensional ODEs by inserting the similarity transformation containing a set of physical parameters. The numerical results are found by using the finite difference method through MATLAB with the help of the shooting technique. The roles of emerging nondimensional numbers/parameters, such as the Darcy number (Da), Prandtl number (Pr), magnetic force parameter ($M$), thermal radiation parameter ($R$), chemical reaction parameter (Kr), and suction parameter ($v_0$), on fluid flow have been observed within the boundary layer. The fluid motion enhances uplifting quantities of radiative parameter and Darcy number. The fluid temperature goes up for growing amounts of thermal radiation and Dufour number. The fluid mass decays to improve the Schmidt number and suction parameter. The local friction coefficient rises about by 32%, 12%, and 15% owing to improving values of Da from 0.5 to 2.0, $R$ from 0.5 to 2.0, and Df from 0.5 to 3.5, respectively. The heat transfer falls down about by 33%, 35% due to enhancing values of $R$ from 0.5 to 2.0, and Df from 0.5 to 3.5, respectively. At last, we looked at our numerical results in relation to previously published articles and discovered that there was a good agreement.

## 1. Introduction

The research of magnetohydrodynamics (MHDs) unrestricted convective heat transmission fluid flow past a vertical surface has attracted much attention because of its potential application in many technological and engineering activities. The velocity profile is transformed when a magnetic field, which is impacted by fluid flow, produces an electromotive force. The direction and intensity of the magnetic field that is being applied have a significant impact on the flow behavior. As a result of the applied magnetic field's control over the suspended particles and changes to their fluid concentration, the flow's properties for heat transmission are unmistakably transmitted. These fluxes can be seen in MHD bearings, MHD pumps, fusion reactors, and generators. Sparrow and Cess [1] explored the impact of a magnetic force on convection heat transmission fluid flow. They also observed the simultaneous action of the induced magnetic field and buoyancy consequence on convective heat transmission in their simulation. Poots [2] has examined the convection flow of a viscous electrically conducting fluid for the influence of the magnetic or electrical fields. Ghosh et al. [3] discussed the impact of an induced magnetic force on convection boundary layer flow past a vertical sheet.

They obtained an exact solution for their simulation. Sarvesan and Singh [4] examined how the incited magnetic field resulting from the velocity of a conducting electrical fluid affected MHD convective fluid flow between two vertical parallel permeable sheets. Furthermore, the consequence of an incited magnetic field over an unstable MHD natural convection flow through a vertical wall has been discussed by Kumar and Singh [5]. They solved coupled nonlinear PDEs by the Crank–Nicolson through the finite difference method. Mohammad et al. [6] recently analyzed the properties of viscous dissipation, thermal radiation, and Joule heating upon MHD radiating nanomaterial viscous flow past a curved sheet together with entropy generation and second-order slip condition. They used the Brownian diffusion and Buongiorno model thermophoresis in their simulation.

In studying space technology and many technical applications, for example, reentry vehicles, in cutting-edge power plants for high-speed flights, processes involving high temperatures, and nuclear rockets, it is vital to consider how heat radiation affects the natural convection flow. When the medium is optically thick, the Rosseland approximation is appropriate. In several investigations involving radiation, this approximation has been employed widely. This approach provides a rough estimate of the radiative heat fluxes for an optically dense medium. Grosan and Pop [7] investigated the impacts of the radiative on the steady fully promoted combined convection flow in a vertical channel. Olanrewaju [8] has studied the effect of the radiative parameter on unstable magnetoconvective heat-mass transport that is traveling through a permeable area. In a first-order chemical reaction, the concentration and reaction rate are directly inversely correlated. Due to numerous kinds of chemical processes occurring with the ambient fluid, the species diffusivity may be absorbed or produced. The attributes and quality of finished products could have a big impact on it. Srinivasa Raju [9] has explained the effects of magnetic fields and chemical reactions on turbulent convective fluid movement traveling through a vertical permeable sheet underneath the effects of thermal diffusion and diffusion-thermo. The effects of radiation parameters and chemical reactions on the 3D MHD incompressible and viscous flow were examined by Sharma and Bhaskar [10]. The Soret–Dufour impact would have also been taken into account in their research work. Shagaiya Daniel et al. [11] clarified the properties of viscous dissipation, thermal radiation, and Joule heating on the time-dependent 2D MHD electrical boundary layer nanofluids' movement over a linear stretching and perforated sheet. To solve the coupled ODEs, they also applied the Keller box approach. The effects of chemical reactions and thermal radiation on the time-dependent MHD convective heat-mass transmission over an infinite porous sheet were very recently examined by Hasanuzzaman et al. [12]. They used the superposition method to solve the governing through MATLAB software.

The relationship between driving fluxes and potentials is really challenging when the phenomena of heat-mass transmission flow are formed simultaneously in liquid motion. In addition to producing the mass flux, the temperature gradient also causes the concentration gradient. The Soret effect is the rate at which mass transfers through temperature differences (thermal diffusion). The Dufour effect, on the other hand, is the rate of heat transmission over a concentration gradient (diffusion-thermo). Such influences were neglected owing to the smaller magnitude of Dufour and Soret's impacts in comparison to Fick's and Fourier's laws. Applications for these effects are prominent in geothermal energy, petrology, hydrology, and nuclear waste disposal, among other fields. The isotope separation method and the mixing of gases with different molecular weights both benefit from thermal diffusion (Soret). Some recent investigations on the Soret and Dufour aspects are mentioned in the studies of [13–19]. The bioconvection phenomenon involving gyrotactic microorganisms in three-dimensional flow dynamics of nanofluid is presented by Awais et al. [20]. Raja et al. [21] presented the convection, second-grade combined convection nanofluid flow associated Cattaneo–Christove heat flux model for viscous dissipation, thermal transportation, and Hall current for high-intensity electric conductive on flow motion and Darcy–Forhheimer law for permeable medium. Recently, Hasanuzzaman et al. [12] examined the properties of chemical reactions and radiative on Hasanuzzaman et al. [17]. Furthermore, the role of the internal heat generation effect on an unstable MHD convection heat-mass transmission flow passing in a vertical permeable sheet has been analyzed by Hasanuzzaman et al. [22]. Hasanuzzaman et al. [23] explored [12] by taking into account the additional term viscous dissipation. Very recently, Hasanuzzaman et al. [23, 24] presented the role of heat absorption or production on time-dependent free MHD convective transport over a vertical porous plate with thermal radiation. They are considered only the uniform porosity in their simulation. Now, we expanded Hasanuzzaman et al.'s study [12] by taking into account the variable porosity of the plate. Their simulation is almost the same as our simulation.

The aforementioned literature study has provided the basis for an analysis of the effects of radiative and variable porosity on an unstable MHD-free convection heat-mass transport traveling over an infinite upright permeable sheet. The main innovation of this research is also heightened by taking into account the variable permeability under the FMD through the shooting technique which is not explained yet. Comparing our findings with those of a previously published paper is another interesting aspect of this paper. Numerous nondimensional parameters and numbers, including the thermal radiation parameter, the Darcy number, the Soret number, the Prandtl number, the Dufour number, the magnetic number, and the Schmidt number, have all been computed. The concentration, velocity, and temperature fields are then graphically observed and analyzed. Moreover, the properties of heat-mass transmission and the local skin friction coefficient have been investigated.

## 2. Problems Design

Let us have a look at an unstable 2D flow of an electrically conducting, incompressible, viscous fluid over an infinitely long, permeable flat sheet that is submerged in a permeable

medium. The infinite verticle sheet is taking on the $x$-axis. This sheet and the free-stream velocity have been considered as parallel to each other. Also, the vertical sheet has been taken into account as normal to the $y$-axis. Transverse to the direction of the flow, a uniformly strong magnetic field $\mathbf{B} = (0, B_0)$ is put into effect. $U_0$ is a velocity where the sheet begins to move impulsively in its own plane. The concentration and temperature are promoted to $C_w$ and $T_w$. Since the plate is infinite, then $\partial u/\partial x \longrightarrow 0$ as $x \longrightarrow \infty$. For this reason, the fluid velocity is a function $y$ and $t$ only.

In comparison to one of the research projects, we assume that the encouraged magnetic field is negligible at quite low flow magnetic Reynolds numbers (Pai, [25]). When this occurs, the magnetic force lines remain stationary concerning the fluid, resulting in $\mathbf{B} = (0, B_0, 0)$. The existing density and the charge continuity equation are given by $\mathbf{J} = (J_x, J_y, J_z)$ and $\nabla.\mathbf{J} = 0$ which suggests that $J_y$ = constant. Only in the $y$-axis direction is the propagation direction assumed. Along the $y$-axis, there is no change in this propagation direction. Therefore, concerning $y$, a derivative of $J_y$ must be zero, that is, as $\partial J_y/\partial y = 0$. Figure 1 shows the coordinate system along with physical model. According to Hasanuzzaman et al. [12], the one-dimensional problem can be expressed as follows using the aforementioned assumptions along with the Boussinesq approximation:

The formula for continuity is as follows:

$$\frac{\partial v}{\partial y} = 0. \tag{1}$$

The equation for momentum is as follows:

$$\frac{\partial u}{\partial t} + v\frac{\partial u}{\partial y} = \upsilon\frac{\partial^2 u}{\partial y^2} + g\beta(T - T_\infty) + g\beta^*(C - C_\infty) - \frac{\sigma' B_0^2 u}{\rho} - \frac{\nu}{K}u. \tag{2}$$

The equation of energy is as follows:

$$\frac{\partial T}{\partial t} + v\frac{\partial T}{\partial y} = \frac{k}{\rho C_p}\frac{\partial^2 T}{\partial y^2} + \frac{D_m k_T}{C_s C_p}\frac{\partial^2 C}{\partial y^2} - \frac{1}{\rho C_p}\frac{\partial q_r}{\partial y}. \tag{3}$$

The concentration formula is as follows:

$$\frac{\partial C}{\partial t} + v\frac{\partial C}{\partial y} = D_m\frac{\partial^2 C}{\partial y^2} + \frac{D_m k_T}{T_m}\frac{\partial^2 T}{\partial y^2} + K'(C - C_\infty). \tag{4}$$

The boundaries Hasanuzzaman et al. [12] are specified by the following equation:

$$t > 0, u = U_0(t), v = v(t), T = T_w, C = C_w \text{ at } y = 0, \tag{5}$$

$$t > 0, u = 0, v = 0, T \longrightarrow T_\infty, C \longrightarrow C_\infty \text{ at } y \longrightarrow \infty, \tag{6}$$

where $g$ = gravitational acceleration, $\beta$ = coefficient of thermal expansion, $C$ = fluid concentration, $\upsilon$ = kinematic viscosity, $v$ = component of the velocity in the $y$-direction, $\rho$ = fluid density, $u$ = component of the velocity in the $x$-direction, $T$ = fluid temperature, $D_m$ = mass diffusivity coefficient, $T_w$ = wall temperature, $K$ = permeability of the porous plate, $q_r$ = component of radiative heat flux, $\beta^*$ = coefficient of concentration expansion, $C_w$ = wall concentration, $T_\infty$ = fluid temperature in the free stream, $C_\infty$ = free stream concentration, $K'$ = chemical reaction rate of spices concentration, $k$ = thermal conductivity of the sheet, $T_m$ = mean temperature of the fluid, $\sigma'$ = electric conductivity, $C_s$ = concentration susceptibility, $k_T$ = thermal diffusion ratio, $C_p$ = specific heat at constant pressure, $\sigma'$ = electric conductivity of spices, and $K'$ = chemical reaction rate.

Using a similarity metric, such as

$$\sigma = \sigma(t), \tag{7}$$

where $\sigma$ is the time-varying length scale. The following length scale is assumed to be the answer to equation (1):

$$v = -v_0\frac{\upsilon}{\sigma}. \tag{8}$$

At the sheet in this instance, the dimensionless normal velocity is $v_0$ while the blowing is represented by $v_0 < 0$ and the suction by $v_0 > 0$.

In accordance with Rosseland approximation (Raptis [26]), the radiative heat flux $q_r$ is as follows:

$$q_r = -\frac{4\sigma^*}{3K^*}\frac{\partial T^4}{\partial y}. \tag{9}$$

Here, $\sigma^*$ and $K^*$ denote the Stefan–Boltzmann constant and mean absorption coefficient, respectively. According to Raptis [27], the temperature differential between the free stream and the fluid is sufficiently modest.

Neglecting higher-order terms when expanding $T^4$ in a Taylor series about $T_0$, we have the following equation:

$$T^4 \cong 4T_0^3 T - 3T_0^4. \tag{10}$$

The following similarity variables are used:

$$\begin{aligned} \eta &= \frac{y}{\sigma}, \\ f(\eta) &= \frac{u}{U_0}, \\ \theta(\eta) &= \frac{T - T_\infty}{T_w - T_\infty}, \\ \phi(\eta) &= \frac{C - C_\infty}{C_w - C_\infty}. \end{aligned} \tag{11}$$

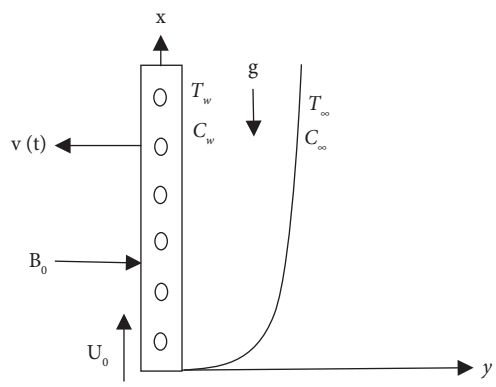


Figure 1: Coordinate system along with physical model.

The equations (1)–(4) are converted into the non-dimensional coupled ODEs listed below using the equations (7)–(11):

$$f''(\eta) + 2\xi f'(\eta) + \mathrm{Gr}\theta(\eta) + \mathrm{Gm}\phi(\eta) - \mathrm{Mf}(\eta) - \frac{1}{\mathrm{Da}} f(\eta) = 0, \tag{12}$$

$$\theta''(\eta) + \frac{\mathrm{Pr}}{1+\mathrm{R}}\{2\xi\theta'(\eta) + \mathrm{Df}\phi''(\eta)\} = 0, \tag{13}$$

$$\phi''(\eta) + 2\xi\mathrm{Sc}\phi'(\eta) + \mathrm{ScSr}\theta''(\eta) + \mathrm{Kr}\phi(\eta) = 0. \tag{14}$$

Then, the altered boundaries that are stated are applied:

$$f(\eta) = 1, \theta(\eta) = 1, \phi(\eta) = 1 \text{ at } \eta = 0, \tag{15}$$

$$f(\eta) = 0, \theta(\eta) = 0, \phi(\eta) = 0 \text{ at } \eta \longrightarrow \infty, \tag{16}$$

where $\mathrm{Da} = K/\sigma^2$ is the Darcy number, the local Grashof number is $\mathrm{Gr} = g\beta(T_w - T_\infty)\sigma^2/U_0\upsilon$, Prandtl number is $\mathrm{Pr} = \rho\upsilon C_p/k$, chemical reaction parameter is $\mathrm{Kr} = K'\sigma^2/\upsilon$, $\mathrm{Gm} = g\beta^*(C_w - C_\infty)\sigma^2/U_0\upsilon$ is the modified local Grashof number, magnetic force parameter is $M = \sigma' B_0^2\sigma^2/\rho\upsilon$, Soret number is $\mathrm{Sr} = D_m k_T(T_w - T_\infty)/\upsilon T_m(C_w - C_\infty)$, Schmidt number is $\mathrm{Sc} = \upsilon/D_m$, Dufour number is $\mathrm{Df} = D_m k_T(C_w - C_\infty)/C_s C_p \upsilon(T_w - T_\infty)$, thermal radiation parameter is $R = 16\sigma^* T_W^2/3K^*K$, and $\xi = \eta + v_0/2$. The Nusselt number (Nu), the skin friction coefficient ($\tau$), and the local Sherwood number (Sh) are the flow parameters and are each defined as follows:

$$\begin{aligned} \mathrm{Nu} &\propto -\theta', \\ \tau &\propto f', \\ \mathrm{Sh} &\propto -\phi'. \end{aligned} \tag{17}$$

## 3. Numerical Solution

The main goal of this investigation is to solve the ODEs (12)–(14) with boundary conditions (15)–(16) using the finite difference method (FDM). This method has been satisfied for accuracy and efficiency in solving various problems (Ali et al. [28] and Cheng and Liu [29]). The solution domain space is discretized in the FMD.

We will apply grid size $\Delta\eta = h > 0$ in $\eta$-direction, $\Delta\eta = 1/N$, with $\eta_i = \mathrm{ih}$ for $i = 0, 1, \ldots, N$. $f_i = f(\eta_i)$, $\theta_i = \theta(\eta_i)$, and $\phi_i = \phi(\eta_i)$ are defined.

At the $i^{\text{th}}$ node, we consider $F_i$, $\Theta_i$, and $\Phi_i$ to be the numerical values of $f, \theta, \text{and } \phi$, respectively. Hence, we suppose the following expressions:

$$\begin{aligned} f'|_i &= \frac{f_{i+1} - f_{i-1}}{2h}, \\ \theta'|_i &= \frac{\theta_{i+1} - \theta_{i-1}}{2h}, \\ \phi'|_i &= \frac{\phi_{i+1} - \phi_{i-1}}{2h}, \end{aligned} \tag{18}$$

$$\begin{aligned} f''|_i &= \frac{f_{i+1} - 2f_i + f_{i-1}}{h^2}, \\ \theta''|_i &= \frac{\theta_{i+1} - 2\theta_i + \theta_{i-1}}{h^2}, \\ \phi''|_i &= \frac{\phi_{i+1} - 2\phi_i + \phi_{i-1}}{h^2}. \end{aligned} \tag{19}$$

By applying FDM, the system of ODES (12)–(14) is discretized in space which is called the main step. To do this, we put (18)–(19) into (12)–(14) and neglect the truncation

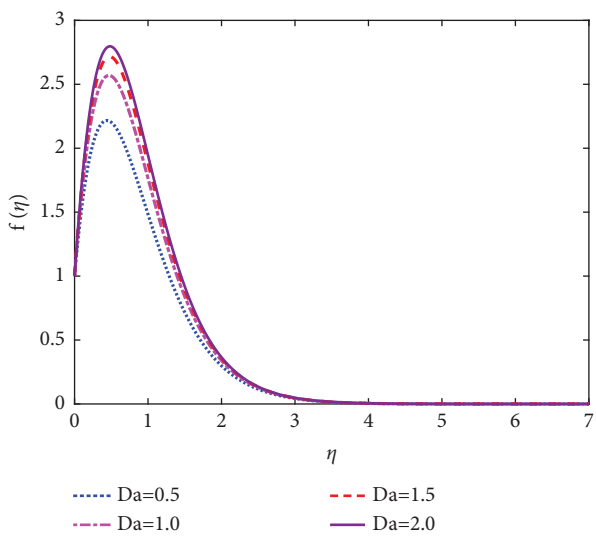


Figure 2: $f(\eta)$ for Da.

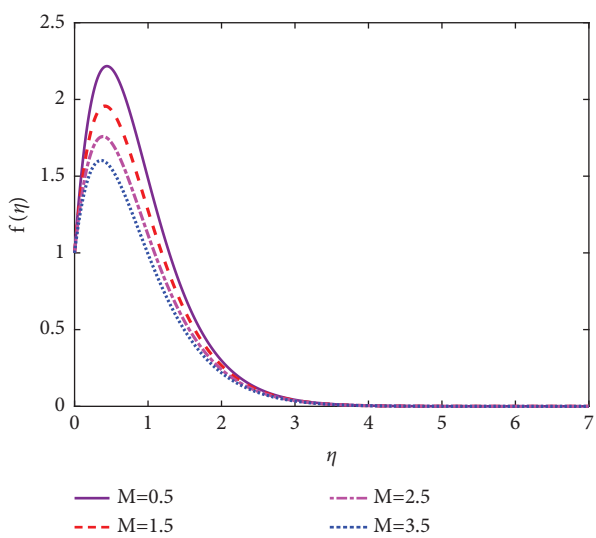


Figure 3: $f(\eta)$ for $M$.

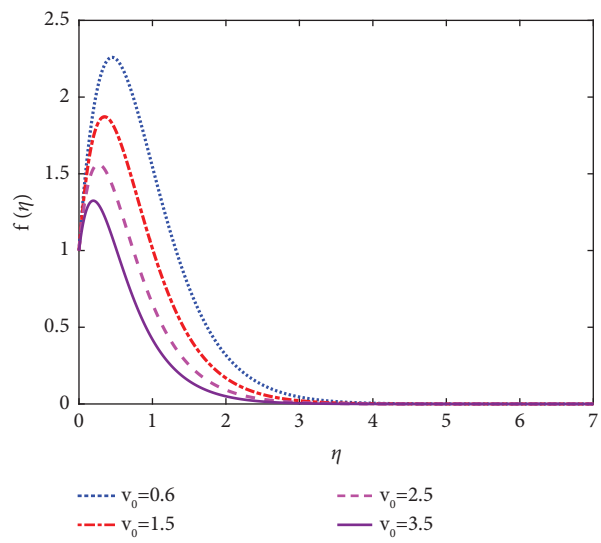


Figure 4: $f(\eta)$ for $v_0$.

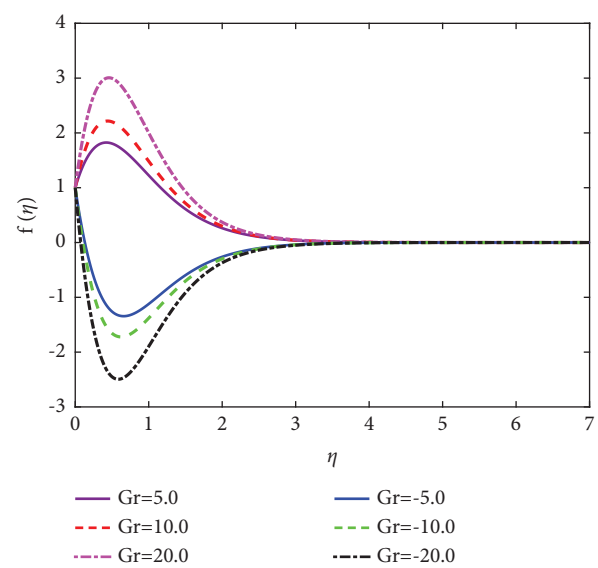


Figure 5: $f(\eta)$ for Gr.

errors. So, following resulting algebraic equations are found for $(i = 0, 1, \ldots, N)$:

$$F_{i+1} - 2F_i + F_{i-1} + \xi h\left(F_{i+1} - F_{i-1}\right) + \mathrm{Gr}\Theta_i + \mathrm{Gm}\Phi_i - \mathrm{Mh}^2 F_i - \frac{1}{\mathrm{Da}} F_i = 0, \tag{20}$$

$$\Theta_{i+1} - 2\Theta_i + \Theta_{i-1} + \frac{\mathrm{Pr}}{1+R}\left[\xi h\left(\Theta_{i+1} - \Theta_{i-1}\right) + \mathrm{Df}\left(\Phi_{i+1} - 2\Phi_i + \Phi_{i-1}\right)\right] = 0, \tag{21}$$

$$\Phi_{i+1} - 2\Phi_i + \Phi_{i-1} + \mathrm{Sc}\left[\xi h\left(\Phi_{i+1} - \Phi_{i-1}\right) + \mathrm{Sr}\left(\Theta_{i+1} - 2\Theta_i + \Theta_{i-1}\right) + \mathrm{Kr}\Phi_i\right] = 0. \tag{22}$$

Also, the boundary conditions are as follows:

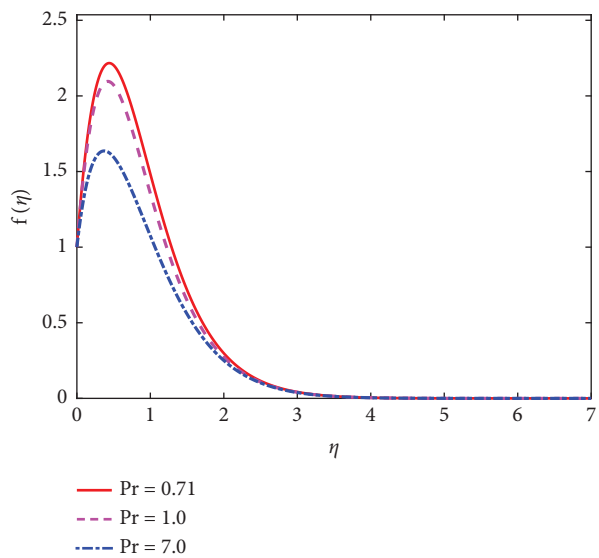


Figure 6: $f(\eta)$ for Pr.

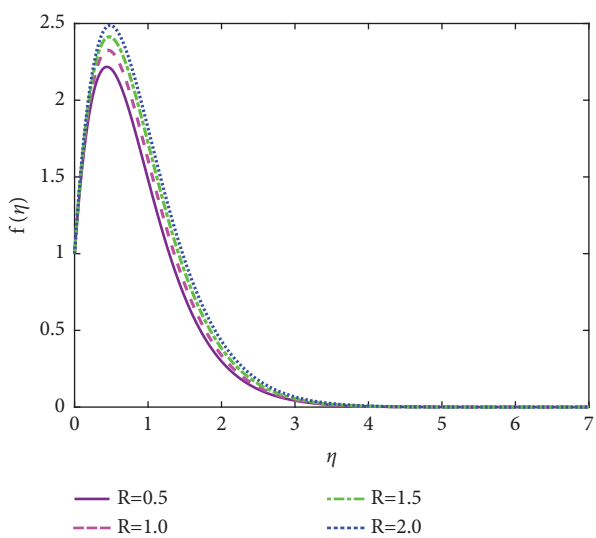


Figure 7: $f(\eta)$ for $R$.

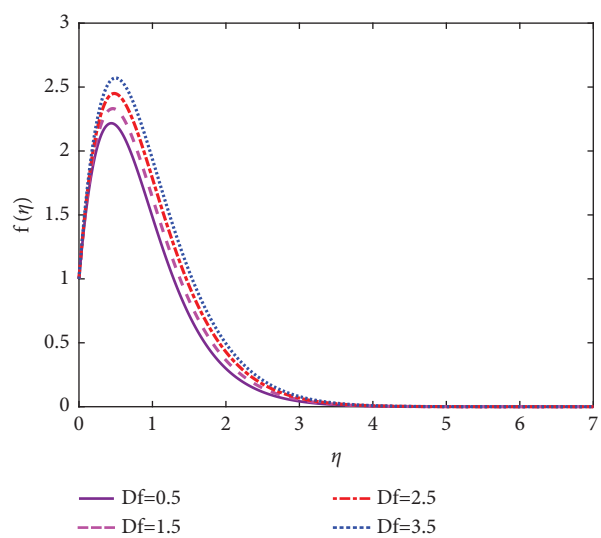


Figure 8: $f(\eta)$ for Df.

$$\begin{aligned} F_0 &= 1, \\ \Theta_0 &= 1, \\ \Phi_0 &= 1, \\ F_N &= 0, \\ \Theta_N &= 0, \\ \Phi_N &= 0. \end{aligned} \tag{23}$$

Equations (20)–(22) represent a nonlinear system of algebraic equations in $F_i, \Theta_i$, and $\Phi_i$. We will apply the Newton iteration method in our calculation using MATLAB software with a suitable initial solution.

## 4. Results and Discussion

This study used numerical analysis to examine the properties of varying porosity and thermal radiation over an unstable MHD convective heat-mass transmission moving through a vertical porous sheet. Using the boundary conditions (15)–(16), the set of ODEs (12)–(14) have been numerically solved using the superposition approach. We also employed the "MATLAB ODE45" program. Figures 2–17 show the impacts of numerous parameters on temperature, concentration, and velocity fields, including the Darcy number (Da), the suction parameter ($v_0$), the radiation parameter ($R$), the Dufour number (Df), the magnetic force parameter

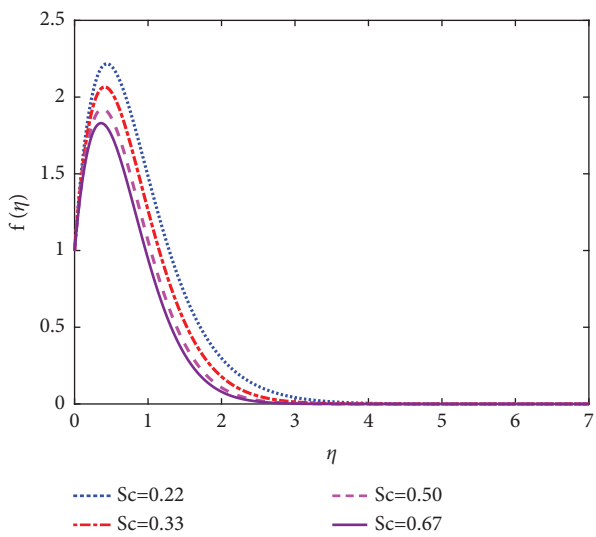


Figure 9: $f(\eta)$ for Sc.

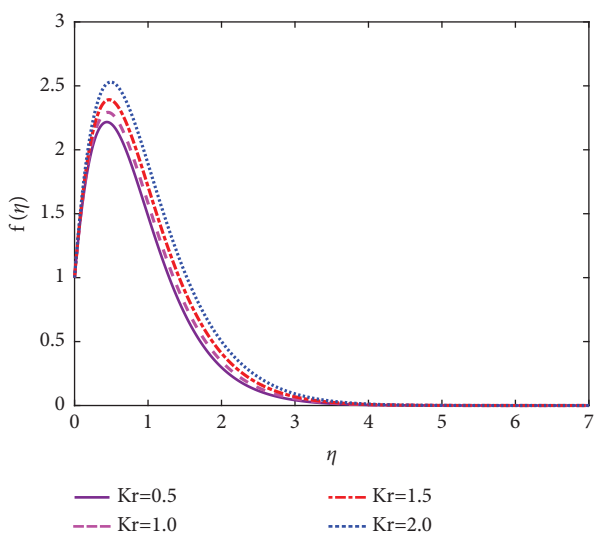


Figure 10: $f(\eta)$ for Kr.

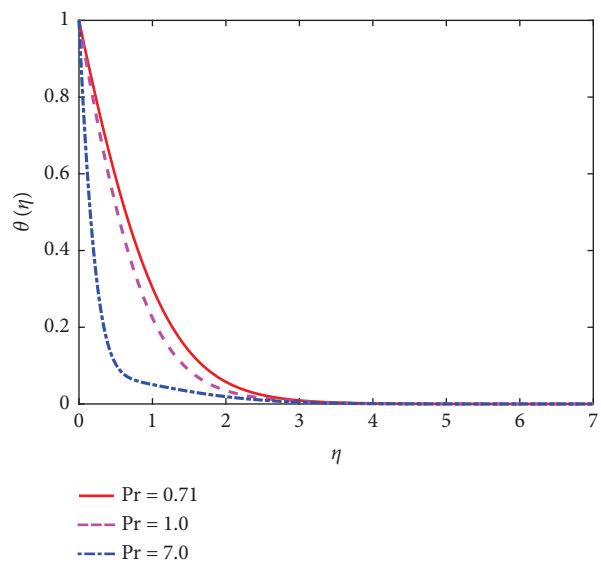


Figure 11: $\theta(\eta)$ for Pr.

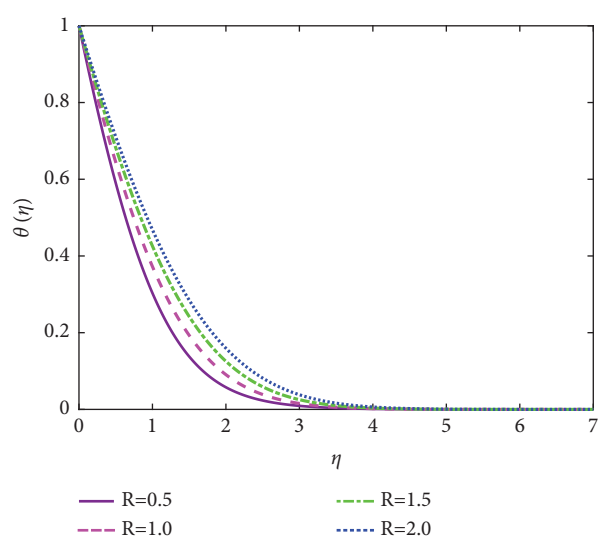


Figure 12: $\theta(\eta)$ for $R$.

($M$), the Schmidt number (Sc), the chemical reaction parameter (Kr), and the Prandtl number (Pr). For Sc, the quantities 0.75, 0.60, and 0.22 are intended (0.60 for vapor water, 0.75 for Oxygen, and 0.22 for Hydrogen). For Pr, the quantities 7.0, 1.0, and 0.71 are also expected (1.0, 7.0 for water at 17° and 0.71 for air at 20°). However, the quantities of the other nondimensional numbers and parameters are chosen at random.

Figures 2–10 portrayed the roles of several nondimensional numbers or parameters on the velocity field ($f(\eta)$). It is observed from equation (12) that the Darcy number (Da) is proportionate to the permeability of the sheet. For larger values of Da, the permeability of the plate is enhanced. Due to this, the fluid motion swiftly accelerates, as shown in Figure 2. Figure 3 demonstrates that at increasing amounts of the magnetic parameter ($M$), the fluid particle's velocity decreases. These results indicate that the magnetic force tends to obstruct the fluid motion. This is because the magnetic force dominates the characteristics of the flow. The velocity of the fluid particle falls quickly for increasing the suction parameter ($v_0$) levels as plotted in Figure 4. The suction means some fluid suck from the computational domain. Then, at increasing levels of $v_0$, the skin friction coefficient drops. So, the fluid cannot travel freely inside the computational domain. The suction parameter demonstrates the well-known concept that suction controls the development of the boundary layer. Due to the increase in Gr, thermal buoyancy forces rise, which results in accelerating the flow rate as shown in Figure 5. The surface is cooling in the case, where Gr is positive and the surface is heating for the positive value of Gr. It is clearly observed from equation (13) that the Prandtl number (Pr) is directly proportionate to the kinematic viscosity ($\nu$). As the amounts of Pr upsurge, then the values of $\nu$ also rises. The fluid particle cannot travel freely in the computational province to

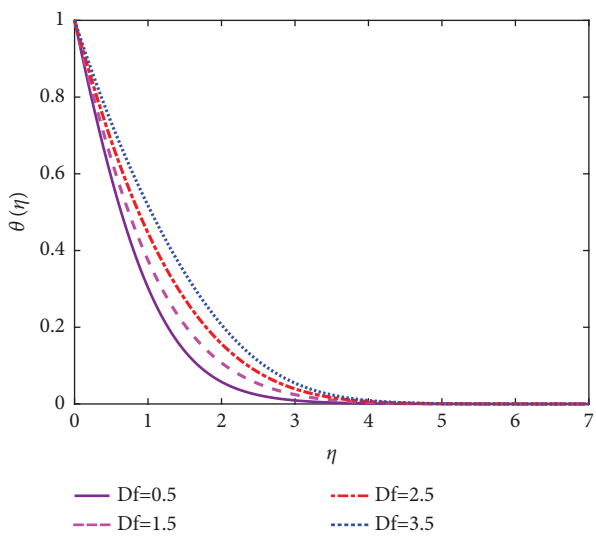


Figure 13: $\theta(\eta)$ for Df.

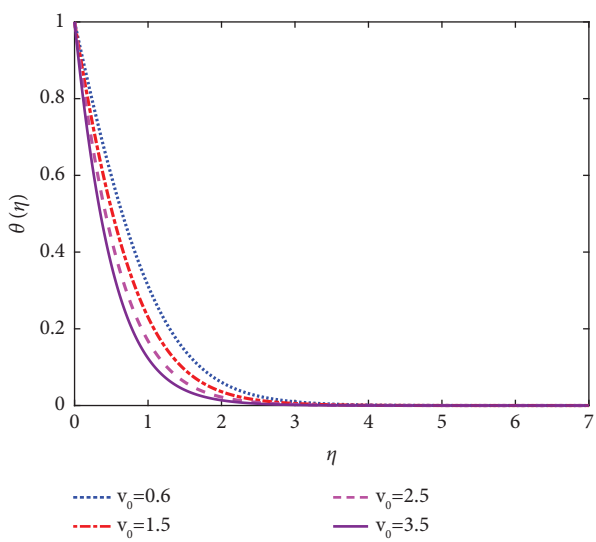


Figure 14: $\theta(\eta)$ for Df.

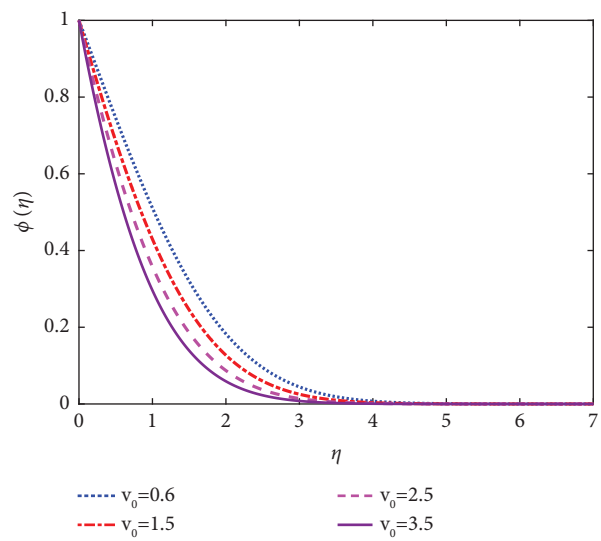


Figure 15: $\phi(\eta)$ for $v_0$.

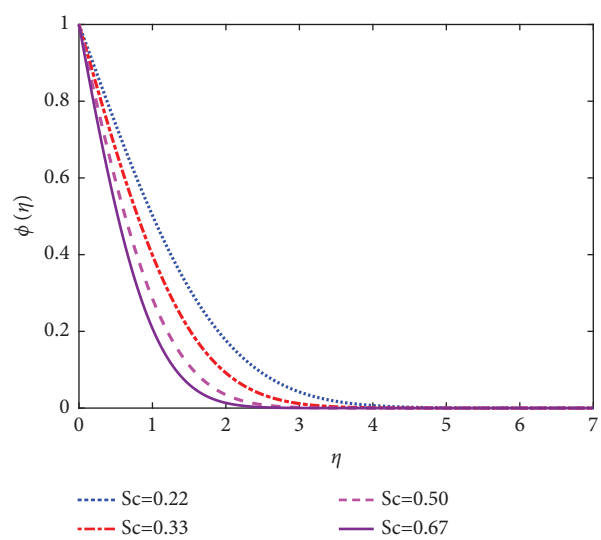


Figure 16: $\phi(\eta)$ for Sc.

improve the values of $\nu$. Therefore, the velocity of the flow decreases in magnitude as Pr improves which is shown in Figure 6. This is because the higher Pr leads to faster cooling of the sheet.

The thermal radiation parameter ($R$) is found to enhance the fluid motion at any point as demonstrated in Figure 7. The higher of the parameter for radiation, the more sharper the enhancement in velocity. Fluid velocity enhances significantly as the Dufour number (Df) increases which is displayed in Figure 8. It is evidently noticed from the mathematical relation of the Dufour number that the fluid viscosity is inversely proportional to the Df. The fluid viscosity decays for growing values of Df. It reveals that the lower frictional is happening in the computational province. Then, the coefficient of skin friction improves for Df. So, the movement of the fluid particle is easy. For this reason, the fluid velocity enhances for Df. It is observed from the equation (14) that the Schmidth number (Sc) is directly proportional to the kinematic viscosity ($\nu$). The values of $\nu$ get better as the Schmidth number rises. So, the strong friction force happens in the computational domain. Since the smaller value of mass diffusivity than momentum diffusivity is predicted for a larger value of Sc. For this reason, the fluid motion decays for growing amounts of Sc as displayed in Figure 9. An increase in the chemical constraint (Kr) primes to a quick enhancement in the velocity as depicted in Figure 10.

Figure 11 demonstrates the thickness of thermal boundary layer for various amounts of Prandtl number (Pr). The temperature gradient at the plate causes the Prandtl number (Pr) to rise, which consequently results in a reduction in the thickness of the thermal boundary layer. As a result, Pr values that are higher result in faster heat transfer

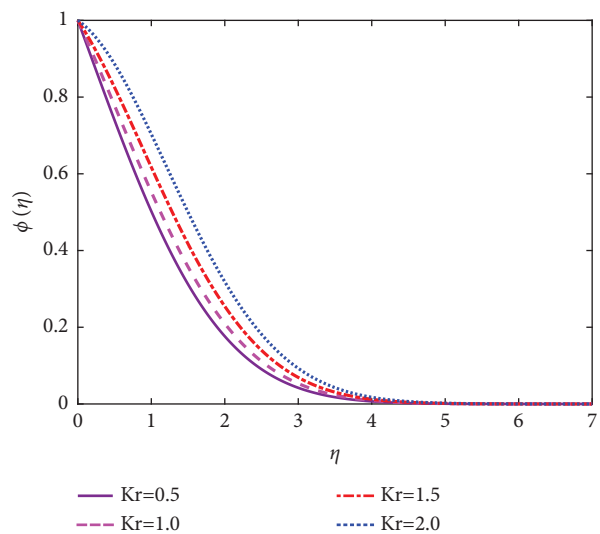


Figure 17: $\phi(\eta)$ for Kr.

Table 1: Computed amounts of $f'(0)$, $\theta'(0)$, and $\phi'(0)$ for several quantities of the Darcy number (Da).

| Da | $f'(0)$ | $-\theta'(0)$ | $-\phi'(0)$ |
|---|---|---|---|
| 0.5 | 6.48609595612254 | 0.912060478723127 | 0.522830028717684 |
| 1.0 | 7.76958496700391 | 0.912060478723127 | 0.522830028717684 |
| 1.5 | 8.28585008753697 | 0.912060478723127 | 0.522830028717684 |
| 2.0 | 8.56316565934878 | 0.912060478723127 | 0.522830028717684 |

Table 2: Computed amounts of $f'(0)$, $\theta'(0)$, and $\phi'(0)$ for several quantities of the magnetic force parameter ($M$).

| $M$ | $f'(0)$ | $-\theta'(0)$ | $-\phi'(0)$ |
|---|---|---|---|
| 0.5 | 6.48609595612254 | 0.912060478723127 | 0.522830028717684 |
| 1.5 | 5.48193224066123 | 0.912060478723127 | 0.522830028717684 |
| 2.5 | 4.66509736510980 | 0.912060478723127 | 0.522830028717684 |
| 3.5 | 3.98049520508116 | 0.912060478723127 | 0.522830028717684 |

Table 3: Computed amounts of $f'(0)$, $\theta'(0)$, and $\phi'(0)$ for several quantities of the Prandtl number (Pr).

| Pr | $f'(0)$ | $-\theta'(0)$ | $-\phi'(0)$ |
|---|---|---|---|
| 0.71 | 6.48609595612254 | 0.912060478723127 | 0.522830028717684 |
| 1.0 | 6.11597522817093 | 1.12073302476402 | 0.522830028717684 |
| 7.0 | 4.30913751459039 | 4.15244127368964 | 0.522830028717684 |

Table 4: Computed amounts of $f'(0)$, $\theta'(0)$, and $\phi'(0)$ for several quantities of the thermal radiation parameter ($R$).

| $R$ | $f'(0)$ | $-\theta'(0)$ | $-\phi'(0)$ |
|---|---|---|---|
| 0.5 | 6.48609595612254 | 0.912060478723127 | 0.522830028717684 |
| 1.0 | 6.79984867269974 | 0.770472135720558 | 0.522830028717684 |
| 1.5 | 7.04314083143484 | 0.677578624619402 | 0.522830028717684 |
| 2.0 | 7.24089718548569 | 0.610895800404981 | 0.522830028717684 |

at the plate. Furthermore, we can infer from the definition that thermal conductivity is inversely proportionate to Pr. When Pr increases, then the thermal conductivity decays. Thus, the heat transmission rates improve for growing amounts of Pr. The fluid temperature drops for Pr as a result. Figure 12 illustrates how decreasing quantities of thermal radiation parameter ($R$) consequences in a diminution in the absolute value of the temperature differential at the wall.

Table 5: Computed amounts of $f'(0)$, $\theta'(0)$, and $\phi'(0)$ for several quantities of the Schmidt number (Sc).

| Sc | $f'(0)$ | $-\theta'(0)$ | $-\phi'(0)$ |
|---|---|---|---|
| 0.22 | 6.48609595612254 | 0.912060478723127 | 0.522830028717684 |
| 0.33 | 6.05639936267642 | 0.912060478723127 | 0.666445200924234 |
| 0.50 | 5.61440393972490 | 0.912060478723127 | 0.861324446082790 |
| 0.67 | 5.30711140750013 | 0.912060478723127 | 1.03742784968807 |

Table 6: Computed amounts of $f'(0)$, $\theta'(0)$, and $\phi'(0)$ for several quantities of the suction parameter ($v_0$).

| $v_0$ | $f'(0)$ | $-\theta'(0)$ | $-\phi'(0)$ |
|---|---|---|---|
| 0.6 | 6.48609595612254 | 0.912060478723127 | 0.522830028717684 |
| 1.5 | 5.99877868195838 | 1.18824335307980 | 0.669673852823192 |
| 2.5 | 5.10676934620164 | 1.52121211071792 | 0.843703745644513 |
| 3.5 | 3.96707694547712 | 1.87456560243411 | 1.02671331838145 |

Table 7: Computed amounts of $f'(0)$, $\theta'(0)$, and $\phi'(0)$ for several quantities of the Dufour number (Df).

| Df | $f'(0)$ | $-\theta'(0)$ | $-\phi'(0)$ |
|---|---|---|---|
| 0.5 | 6.48609595612254 | 0.912060478723127 | 0.522830028717684 |
| 1.5 | 6.80650748695306 | 0.804916333048873 | 0.522830028717684 |
| 2.5 | 7.12691901773141 | 0.697772187373568 | 0.522830028717684 |
| 3.5 | 7.44733054856885 | 0.590628041695732 | 0.522830028717684 |

Therefore, when $R$ increases, the heat transmission rates at the wall decline. As a result, the temperature field gets better as $R$ increases. The thermal boundary has thickened as a result of the radiative parameter. The system cools as a result of the fluid being able to discharge the heat energy from the flow area. This is because the enhanced temperature field produced by the Rosseland approximation. The Dufour effect deals with the heat flow caused by a concentration (solutal) gradient. It is well known from the equation (13) that the Dufour number (Df) is directly proportional to the thermal conductivity. Growing thermal conductivity ratings result in a slower rate of heat transmission. Hereafter, the temperature of fluid augmented owing to improving values of Df as illustrated in Figure 13. In contrast to when the Dufour effect is absent, the temperature field is higher when Df is present. In the presence of potent Df effects, the thermal boundary layer thickness accelerates noticeably.

From Figure 16, it is detected a decay in the concentration field with the variable of similarity $\eta$ for all amounts of Sc. The Schmidt number has an inverse relationship to the rate of molecule diffusion, as shown by the mathematical of Sc. It implies that for increasing levels of Sc, the mass transfer rate rapidly increases. A rise in Sc produces a reduction the mass rates in the thickness of boundary layer, resulting in the concentration field diminishing. It is interpreted from Figure 17 that in the existence of the chemical reaction ($\mathrm{Kr} \neq 0$), the fluid concentration enhances rapidly in comparison with $\mathrm{Kr} = 0$. It is also explored that an increment in Kr goes up the concentration field within the boundary layer. So, the mass transfer boundary layer thickness improves. This happens because flow consumes the chemical in the chemical reaction process, resulting in acceleration in the concentration field.

Tables 1–7 demonstrate the properties of the dimensionless parameters on the values of $f'(0)$, $\theta'(0)$, and $\phi'(0)$. The coefficient of skin friction ($f'(0)$) enhances for growing amounts of Da, $R$, and Df. Besides this, the opposite performance is noticed for growing amounts Pr, $v_0$, $M$, and Sc. The values of $f'(0)$ enhance about by 32%, 12%, and 15% owing to improving values of Da from 0.5 to 2.0, $R$ from 0.5 to 2.0, and Df from 0.5 to 3.5, respectively. For this reason, the fluid velocity goes up quickly for these parameters. While, improving values of $M$ from 0.5 to 3.5, Pr from 0.71 to 7.0, Sc from 0.22 to 0.67, $v_0$ from 0.6 to 3.5 and the values of $f'(0)$ diminish 39%, 34%, 18%, and 39%, respectively. As a result, the fluid motion reduces in this situation. The heat transmission rate ($\theta'(0)$) decays for elevating amounts of $R$ and Df. For this reason, the fluid temperature is enhanced for this case. On the other hand, the inverse tendencies are found for $v_0$ and Pr. The values of $\theta'(0)$ fall down about by 33%, and 35% due to enhancing values of $R$ from 0.5 to 2.0, and Df from 0.5 to 3.5, respectively. Besides, the rising values of $v_0$ from 0.6 to 3.5, and Pr from 0.71 to 7.0, the values of $\theta'(0)$ go up about by 105% and 355%, respectively. Finally, The mass transmission rate accelerates for affecting the Schmidth number (sc) and the suction parameter ($v_0$). The mass transmission rate enhances around by 98%, and 96% owing to improving values of Sc from 0.22 to 0.67, and $v_0$ from 0.6 to 3.5, respectively. Hence, the fluid concentration decays in this case.

## 5. Comparable Tables

The numerical result of the existing research has been compared with previously published work which is included in Tables 8 and 9. Numerical outcomes for the amounts of

Table 8: Values of $-\theta'(0)$ and $-\varphi'(0)$ for $v_0$ and Df.

| $v_0$ | Df | $-\theta'(0)$ Hasanuzzaman et al. [17] | $-\theta'(0)$ Present study | $-\varphi'(0)$ Hasanuzzaman et al. [17] | $-\varphi'(0)$ Present study |
|---|---|---|---|---|---|
| 0.5 | 0.2 | 1.41983 | 1.49929 | 0.22187363 | 0.19355095030467 |
| 0.5 | 0.5 | 1.48232 | 1.36665 | 0.13702065 | 0.13355095030862 |

Table 9: Values of $-\theta'(0)$ and $-\varphi'(0)$ for Pr and Sc.

| Pr | Sc | $-\theta'(0)$ Hasanuzzaman et al. [17] | $-\theta'(0)$ Present study | $-\varphi'(0)$ Hasanuzzaman et al. [17] | $-\varphi'(0)$ Present study |
|---|---|---|---|---|---|
| 0.71 | 0.22 | 1.40316 | 1.39423 | 0.24471 | 0.26012 |
| 1.0 | 0.22 | 1.82297 | 1.83429 | 0.28981 | 0.27012 |
| 0.71 | 0.60 | 1.41983 | 1.39666 | 0.22187 | 0.17355 |

the heat transmission rate at the plate are compared with the findings of Hasanuzzaman et al. [12] for the special case of uniform porosity to confirm the validity and correctness of the result obtained.

## 6. Conclusions

Applying the FDM to the motion of a time-dependent 2D viscous, electrically conducting, and incompressible fluid over an infinite upright permeable sheet, one can resolve the transform governing equations for variable porosity and thermal radiation over MHD flow. The momentous remarks of this research are as follows:

(i) The fluid motion and its boundary layer thickness come into a restraint as improving the suction, magnetic field, Schmidth number, and Prandtl number for distinct values are upgraded

(ii) The fluid motion will be enhanced for the distinct standards of the Darcy number, thermal radiation parameter, Dufour number, and chemical reaction

(iii) The fluid temperature improves as the thermal radiation and Dufour number escalate

(iv) The concentration of the fluid decays as the suction and Schmidth number improve

(v) The local friction coefficient increases about by 32%, 12%, and 15% owing to improving values of Da from 0.5 to 2.0, $R$ from 0.5 to 2.0, and Df from 0.5 to 3.5, respectively

(vi) The heat transfer falls down about by 33%, and 35% due to enhancing values of $R$ from 0.5 to 2.0, and Df from 0.5 to 3.5, respectively

(vii) The mass transmission rate develops around by 98%, and 96% owing to growing amounts of Sc from 0.22 to 0.67, and $v_0$ from 0.6 to 3.5, respectively

The outcome of this study could be useful in a variety of fields, including metallurgy, geothermal energy extraction, petroleum and mining engineering, chemical technology, solar and wind power, plasma studies, paper manufacture, furnace design, suspensions, thermonuclear fusion, and more.

## Nomenclature

$u$: $x$-axis velocity component ($ms^{-1}$)
MHD: Hydromagnetic
$J$: Density of current ($Am^{-2}$)
$T_w$: Wall temperature ($kg{\cdot}m^2{\cdot}s^{-2}{\cdot}K^{-1}$)
$C$: Concentration of the fluid (mol. $m^{-3}$)
$C_\infty$: Free stream concentration
$U_0(t)$: Uniform surface velocity ($ms^{-1}$)
$g$: Acceleration due to gravity ($ms^{-2}$)
$\beta$: Volumetric expansion coefficient with temperature
$k$: Thermal conductivity ($Wm^{-1}K^{-1}$)
$C_p$: Specific heat at constant pressure
$k_T$: Thermal diffusion ratio ($m^2s^{-1}$)
$\sigma$: Similarity parameter
Gr: Local Grashof number
$M$: Magnetic parameter
Df: Dafour number
Sc: Schmidt number
$\tau$: Coefficient of the local skin friction
Sh: Sherwood number
$\theta(\eta)$: Dimensionless temperature
$q_r$: Radiative heat flux ($Js^{-1}$)
$R$: Thermal radiation parameter
$v$: $y$-axis velocity component ($ms^{-1}$)
$B$: Uniform magnetic field ($Am^{-1}$)
$T$: The temperature of fluid ($kg{\cdot}m^2{\cdot}s^{-2}{\cdot}K^{-1}$)
$T_\infty$: Free stream temperature
$C_w$: Concentration of the wall (mol. $m^{-3}$)
$\rho$: Fluid density ($MV^{-1}$)
$v(t)$: Suction velocity ($ms^{-1}$)
$\upsilon$: Kinematic viscosity ($m^2s^{-1}$)
$\beta^*$: Volumetric expansion coefficient with concentration
$C_s$: Concentration susceptibility
$T_m$: Fluid mean temperature
$D_m$: Coefficient of mass diffusivity
$v_0$: Blowing and suction

Gm: Modified local Grashof number
Pr: Prandtl number
Sr: Soret number
t: Time (s)
Nu: Nusselt number
$f'(\eta)$: Dimensionless velocity
$\phi(\eta)$: Dimensionless concentration
$K'$: Chemical reaction rate of concentration
Kr: Chemical reaction parameter.

## Data Availability

The datasets generated and analysed during the current study are not publicly available due to continuous studying but are available from the corresponding author on reasonable request.

## Conflicts of Interest

The authors declare that they have no conflicts of interest.

## References

[1] E. M. Sparrow and R. D. Cess, "The effect of a magnetic field on free convection heat transfer," *International Journal of Heat and Mass Transfer*, vol. 3, no. 4, pp. 267–274, 1961.

[2] G. Poots, "Laminar natural convection flow in magnetohydrodynamics," *International Journal of Heat and Mass Transfer*, vol. 3, no. 1, pp. 1–25, 1961.

[3] S. K. Ghosh, O. Anwar Bég, and J. Zueco, "Hydromagnetic free convection flow with induced magnetic field effects," *Meccanica*, vol. 45, no. 2, pp. 175–185, 2010.

[4] Sarveshanand and A. K. Singh, "Magnetohydrodynamic free convection between vertical parallel porous plates in the presence of induced magnetic field," *SpringerPlus*, vol. 4, pp. 333–413, 2015.

[5] A. Kumar and A. K. Singh, "Unsteady MHD free convective flow past a semi-infinite vertical wall with induced magnetic field," *Applied Mathematics and Computation*, vol. 222, pp. 462–471, 2013.

[6] R. Muhammad, M. I. Khan, N. B. Khan, and M. Jameel, "Magnetohydrodynamics (MHD) radiated nanomaterial viscous material flow by a curved surface with second order slip and entropy generation," *Computer Methods and Programs in Biomedicine*, vol. 189, Article ID 105294, 2020.

[7] T. Grosan and I. Pop, "Thermal radiation effect on fully developed mixed convection flow in a vertical channel," *Technische Mechanik-European Journal of Engineering Mechanics*, vol. 27, no. 1, pp. 37–47, 2007.

[8] P. O. Olanrewaju, "Unsteady three-dimensional MHD flow and mass transfer in a porous space in the presence of thermal radiation," *World Applied Sciences Journal*, vol. 2, no. 2, pp. 044–051, 2012.

[9] R. Srinivasa Raju, "Combined influence of thermal diffusion and diffusion thermo on unsteady MHD free convective fluid flow past an infinite vertical porous plate in presence of chemical reaction," *Journal of the Institution of Engineers: Series C*, vol. 97, no. 4, pp. 505–515, 2016.

[10] K. Sharma and K. Bhaskar, "Influence of Soret and Dufour on three-dimensional MHD flow considering thermal radiation and chemical reaction," *International Journal of Algorithms, Computing and Mathematics*, vol. 6, no. 1, pp. 3–17, 2020.

[11] Y. Shagaiya Daniel, Z. Abdul Aziz, Z. Ismail, and F. Salah, "Effects of thermal radiation, viscous and Joule heating on electrical MHD nanofluid with double stratification," *Chinese Journal of Physics*, vol. 55, no. 3, pp. 630–651, 2017.

[12] M. Hasanuzzaman, T. Ahamed, and A. Miyara, "Thermal radiation effect on unsteady magneto-convective heat-mass transport passing in a vertical permeable sheet with chemical reaction," *Computational and Mathematical Methods in Medicine*, vol. 2022, Article ID 2872940, 11 pages, 2022.

[13] T. Hayat, I. Ullah, T. Muhammad, and A. Alsaedi, "Radiative three-dimensional flow with Soret and Dufour effects," *International Journal of Mechanical Sciences*, vol. 133, pp. 829–837, 2017.

[14] J. Wang, M. Yang, Y. L. He, and Y. Zhang, "Oscillatory double-diffusive convection in a horizontal cavity with Soret and Dufour effects," *International Journal of Thermal Sciences*, vol. 106, pp. 57–69, 2016.

[15] D. Pal and S. Chatterjee, "Soret and Dufour effects on MHD convective heat and mass transfer of a power-law fluid over an inclined plate with variable thermal conductivity in a porous medium," *Applied Mathematics and Computation*, vol. 219, no. 14, pp. 7556–7574, 2013.

[16] S. Qayyum, M. I. Khan, T. Hayat, and A. Alsaedi, "A framework for nonlinear thermal radiation and homogeneous-heterogeneous reactions flow based on silver-water and copper-water nanoparticles: a numerical model for probable error," *Results in Physics*, vol. 7, pp. 1907–1914, 2017.

[17] M. Hasanuzzaman, M. Azad, M. M. Hossain, and M. Hossain, "Effects of Dufour and thermal diffusion on unsteady MHD free convection and mass transfer flow through an infinite vertical permeable sheet," *SN Applied Sciences*, vol. 3, no. 12, pp. 882–911, 2021.

[18] B. K. Sharma, S. Gupta, V. V. Krishna, and R. J. Bhargavi, "Soret and Dufour effects on an unsteady MHD mixed convective flow past an infinite vertical plate with Ohmic dissipation and heat source," *Afrika Matematika*, vol. 25, no. 3, pp. 799–821, 2014.

[19] M. S. Alam, M. M. Rahman, and M. A. Samad, "Dufour and Soret effects on unsteady MHD free convection and mass transfer flow past a vertical porous plate in a porous medium," *Nonlinear Analysis Modelling and Control*, vol. 11, no. 3, pp. 217–226, 2006.

[20] M. Awais, S. Ehsan Awan, M. A. Z. Raja et al., "Heat transfer in nanomaterial suspension (CuO and Al2O3) using KKL model," *Coatings*, vol. 11, no. 4, p. 417, 2021.

[21] M. A. Z. Raja, Z. Khan, S. Zuhra et al., "Cattaneo-christov heat flux model of 3D hall current involving biconvection nanofluidic flow with Darcy-Forchheimer law effect: back-propagation neural networks approach," *Case Studies in Thermal Engineering*, vol. 26, Article ID 101168, 2021.

[22] M. Hasanuzzaman, S. Sharin, T. Hassan, M. A. Kabir, R. Afroj, and A. Miyara, "Unsteady magneto-convective heat-mass transport passing in a vertical permeable sheet with internal heat generation effect," *Transport Engineer*, vol. 9, Article ID 100126, 2022.

[23] M. Hasanuzzaman, S. Akter, S. Sharin, M. M. Hossain, A. Miyara, and M. A. Hossain, "Viscous dissipation effect on unsteady magneto-convective heat-mass transport passing in

a vertical porous plate with thermal radiation," *Heliyon*, vol. 9, no. 3, Article ID 14207, 2023.

[24] M. Hasanuzzaman, M. A. Labony, and M. M. Hossain, "Heat generation and radiative effects on time-dependent free MHD convective transport over a vertical permeable sheet," *Heliyon*, vol. 9, no. 10, Article ID 20865, 2023.

[25] S. I. Pai, "Magnetogasdynamics and electromagnetogasdynamics," in *Magnetogasdynamics and Plasma Dynamics*, pp. 27–40, Springer Vienna, Vienna, Austria, 1962.

[26] A. Raptis, "Flow of a micropolar fluid past a continuously moving plate by the presence of radiation," *International Journal of Heat and Mass Transfer*, vol. 41, no. 18, pp. 2865-2866, 1998.

[27] A. Raptis, "Radiation and viscoelastic flow," *International Communications in Heat and Mass Transfer*, vol. 26, no. 6, pp. 889–895, 1999.

[28] J. C. Ali, E. A. Sameh, and S. A. Abdulkareem, "Melting and radiation effects on mixed convection from a vertical surface embedded in a non-Newtonian fluid saturated non-Darcy porous medium for aiding and opposing eternal flows," *International Journal of the Physical Sciences*, vol. 5, no. 7, pp. 1212–1224, 2010.

[29] W. T. Cheng and C. H. Lin, "Unsteady mass transfer in mixed convective heat flow from a vertical plate embedded in a liquid-saturated porous medium with melting effect," *International Communications in Heat and Mass Transfer*, vol. 35, no. 10, pp. 1350–1354, 2008.